LOOK ACADEMIC PUBLISHERS
OPEN ACCESS

INTERNATIONAL JOURNAL OF ENVIRONMENTAL & SCIENCE EDUCATION
2016, VOL. 11, NO. 18, 11721-11733

A Low Emission Axial-Flow Turbine for the Utilization of Compressible Natural Gas Energy in the Gas Transport System of Russia

Gennadiy Rakov, Viktor Rassokhin, Nikolay Zabelin, Sergey Olennikov, Aleksandr Sebelev, Aleksandr Sukhanov, and Sergey Schislyaev

Peter the Great Saint-Petersburg Polytechnic University,
Department of Turbines, Hydromachines and Aero-engines, Saint-Petersburg, RUSSIA.

ABSTRACT

Natural gas deposits and a developed gas transport system (GTS) infrastructure of Russia are a national treasure that makes the country a leader in extraction and supply of natural gas – the cleanest type of fossil fuel. The operation of the GTS has a direct effect on energy, social, and economic security; in addition, Russia is the main supplier of gas to European countries. Therefore, the modernization of the GTS is one of the main directions of governmental work. This research investigates an expansion turbine for the trigger of a significant pressure drop at a low volume flow of natural gas with an electrical power of 1 kW, which is manufactured by 3D printing the plastic parts of the turbine. The study was conducted under a federal program titled “Research and Development in Priority Directions for the Development of the Scientific and Technological Complex of Russia in 2014-2020”. The research used the analytical method and mathematical calculation method. The validity of obtained results was achieved by using the ANSYS WB software. The results showed that using abutting contact shoulders in a plastic disc enables reducing the maximum stress in this disc by more than 25%.

KEYWORDS
Gas transport system of Russia; expansion turbine; one-sheet hyperboloid of revolution; plastic disc; gas transport system modernization

ARTICLE HISTORY
Received 5 May 2016
Revised 18 September 2016
Accepted 6 October 2016

Introduction

The GTS uses both centralized power supply and other power sources, including renewable ones. Power is supplied to the GTS at terminal points: gas distribution stations (GDS), gas distribution plants (GDP), and gas distribution boxes (GDB) (Hagan, 2015; Martens & Behrens, 2014; Pavel et al., 2016). Presently, the main technique used to convert gas pressure in main pipelines into consumption system pressure is gas expansion (Yang et al., 2016; Imboccioli & Bernardi, 2016; Hill & Hill, 2016). At that, gas expansion energy is lost entirely (Ogawa et al., 2016; Příhoda et al., 2016; Xu et al., 2015). This energy

CORRESPONDENCE Sergey Schislyaev sms1947@mail.ru

could and should be converted into mechanical energy at the turbine generator shaft and subsequently converted into electrical energy for consumer needs.

This study on the design of turbine generators for said purposes was conducted under a federal target program titled “Research and Development in Priority Directions for the Development of the Scientific and Technological Complex of Russia in 2014-2020” – CONTRACT No. 14.578.21.0127 on the provision of a grant from the federal budget for the conduction of applied studies and experimental design on the subject “Design and Manufacturing of Turbo Generation Installations with an electrical power of 1 and 3 kW that use compressible natural gas energy for the gas transport system of Russia” (application code “2015-14-579-0173-141”). Applied study and experimental design unique identifier RFMEFI57815X0127 (Kuklina et al., 2015; Kushchenko et al., 2015; Shipovalov et al., 2015).

In accordance with the task of the federal target program, an expansion turbine for the trigger of a significant pressure drop at a low volume flow of natural gas with an electrical power of 1 kW, manufactured by 3D printing the plastic parts of the turbine, was designed. Using plastic instead of steel to manufacture the set of nozzles (SN) and turbine wheel necessitates the search for construction schematics that would provide for the strength and reliability of respective parts of high-pressure-drop and low emission turbines (LET), as well as cost parameters.

Preliminary studies on the current state of turbine engineering found extensive experience of design and operation of heavy loaded active axial stages with axially symmetric nozzles in turbo-pump assemblies in modern jet engines, electric power installations in submersible vehicles, feed-pumps of steam turbines, and control stages of high-capacity steam turbines with multiple steam nozzle control (Khaleghi et al., 2013; Timm et al., 2013; Yao et al., 2013). The simplicity and reliability of this class of turbines determines the need to use active axial stages in expansion turbo generators.

Aim of the Study

This study aims to design an expansion turbine for the trigger of a significant pressure drop at a low volume flow of natural gas with an electrical power of 1 kW.

Research questions

What are the principles for the design of a turbine stage flow range?

Method

The theoretical and methodological framework of this research included the theory of regulation of sustainable development of a gas transport system under integrative processes of economic development, as well as theories of Russian and foreign experts in the field of engineering.

A set of methods relevant to the studied problem was used to achieve the set goal. These included the generalization of domestic and foreign experience, abstract-logical and analytical methods, analysis, and synthesis. The validity of mathematical calculations was achieved by using the ANSYS WB software.

Data, Analysis, and Results

Optimization calculations determined the geometric and gas-dynamic characteristics of the turbine stage in its conventional design – Cv stage, Figure 1. The stage has a set of axially symmetric nozzles and a wheel with a shroud. The flowchart of the stage flow range and the main geometric characteristics of the turbine stage are presented in Figure 3.

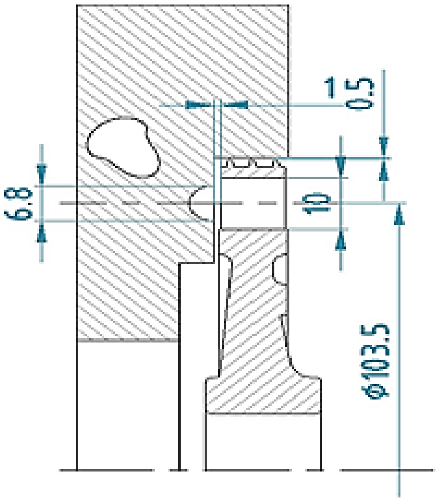

Figure 1. Conventional turbine Cv stage.

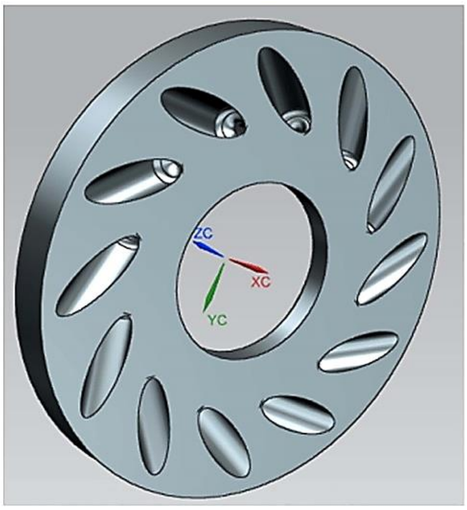

Figure 2. 3D model of the set of nozzles in the Cv stage.

The 3D model of the SN of the stage is presented in Figure 2. Obviously, supplying the working mass (WM) to this SN in the axial direction will be less effective than the tangential supply via a circular or "scroll" connecting pipe. Indeed, in the SN under consideration, with axial supply, the WM has to make a (90°-α1=70°) turn, while with tangential movement – a 34° turn. Furthermore, when flowing around the sharp edges of the root of the nozzle inlet ellipse (Figure 2), the flow has a complex spatial structure, which generates eddy zones directly at the inlet of the shaped subsonic nozzle section. Tangential WM movement reduces the turn angle at the inlet and the eddy zones before the subsonic nozzle section; however, the construction of the SN inlet remains suboptimal due to the elongated bevel cut of the nozzle at the SN entrance. At that, the bigger the cut, the smaller the nozzle angle α1.

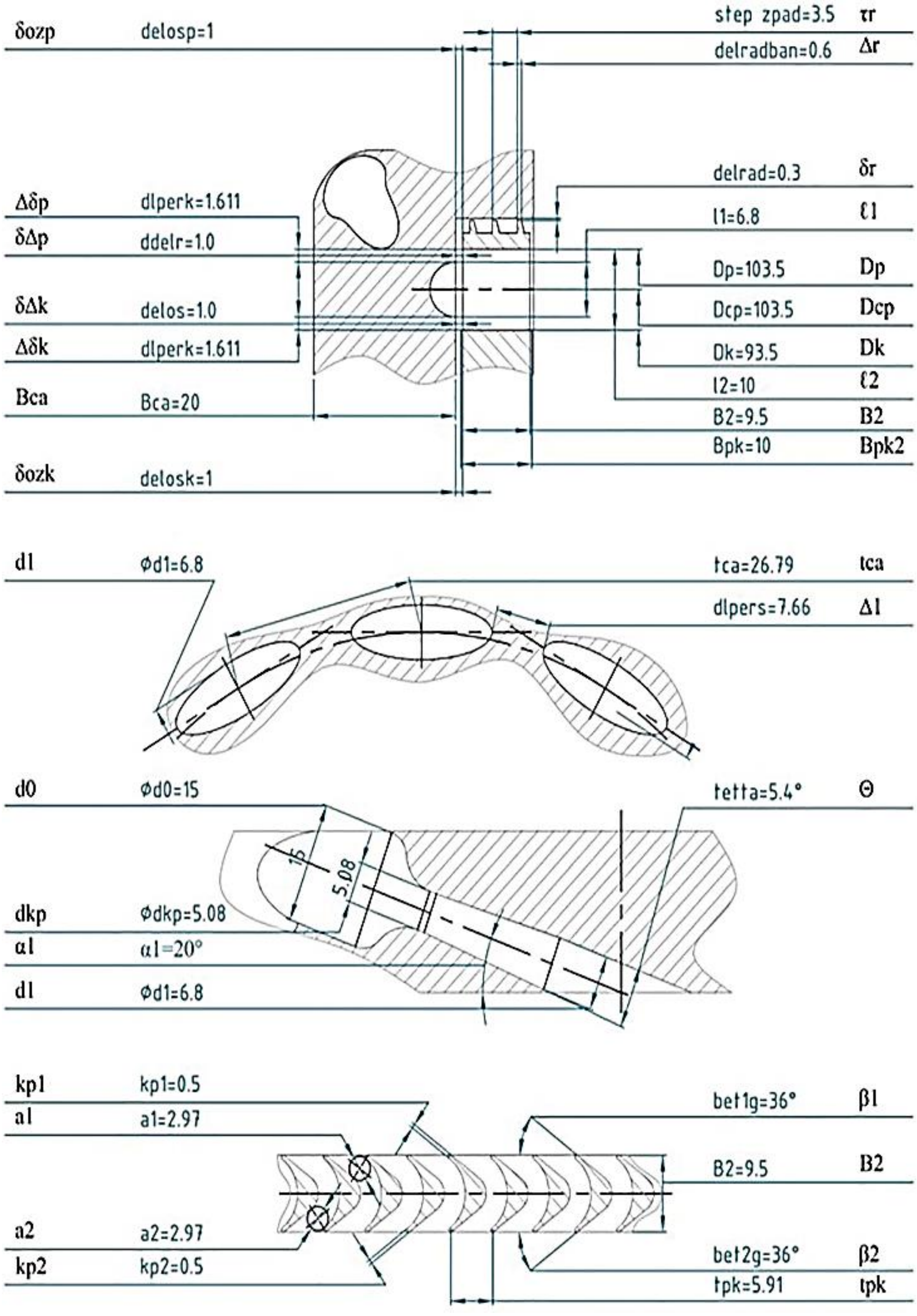

Figure 3. Stage flow range.

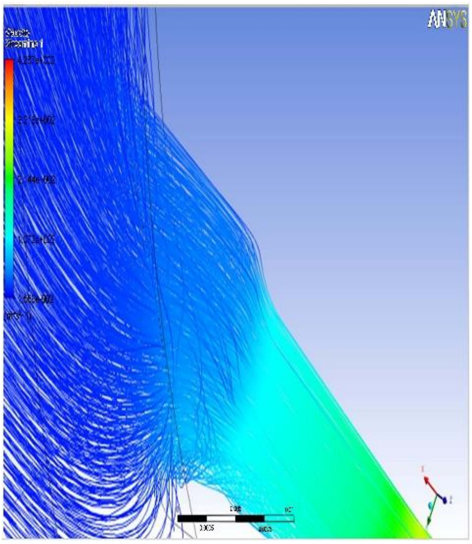

Figure 4. 3D visualization of the flow.

Consider that the axes of nozzles are rectilinear and, thus, belong to one plane – a one-sheet hyperboloid of revolution.

(OSHR) (Kirillov, 1972). the neck whereof, according to classical shaping, is located in the pitch diameter of the nozzle outlet. Consequently, at the nozzle inlet, the flow should have a respective radial component. To that end, study (Rassokhin, 2004) offers to "open" the SN above the shaped nozzle inlet and to locate the open flow area of the inlet above them. Experimental and computation studies demonstrated in research (Rakov, 1982) confirmed the advantages of the new design of the SA inlet in comparison to the Cv variant.

Figure 5. 3D model of the SN in the modernized stage – CvMR.

At the Peter the Great St. Petersburg Polytechnic University Turbines, Hydro Machines and Aircraft Engines department, work is done, led by Professor Rassokhin V.A. and Associate Professor Rakov G.L., to design low emission turbines of a new class, including through the modernization of conventional axial stages of low emission turbines with axially symmetric nozzles. Three-dimensional gas-dynamic calculations in the ANSYS CA software with a modernized inlet showed minimum kinetic energy loss at the nozzle inlet, which is caused by the fact that virtually no eddy zones are generated during tangential WM movement in the circular connecting pipe. The analysis of the SN inlet presented in (Rakov, 1982) and new experience gained during the computer simulation of flows at the SN inlet enabled developing a new principle of designing the SN inlet (Figure 4 and Figure 5).

The SN of a modernized CvMR stage with an inlet designed according to the recommendations of (Rakov, 1982) is presented in Figure 5. The stage wheel has the same geometry as that of the Cv stage.

Problems related to the hyperbolic flow of the WM and, consequently, the presence of radial velocity components also occur at the wheel outlet. It is worth noting that problems that occur in the axial clearance of the stage are more serious than the ones at the SN inlet due to high supersonic flow velocities in high-drop stages and peripherally directed radial velocities, which increase the leakage of the WM into the radial clearance. WM leaks will increase with the reduction of the nozzle angle α1 and the increase in the axial clearance size, which depends on both unsteady phenomena in the axial clearance and thermal expansion of the turbine construction elements. Certain difficulties are caused by the extension of the beveled cut of the nozzle during the reduction of the α1 angle, which necessitates increasing the upper overlap of wheel blades, thus causing increased convection loss. A simple method is offered for the spatial shaping of the flow range of the main stage elements (Figure 6).

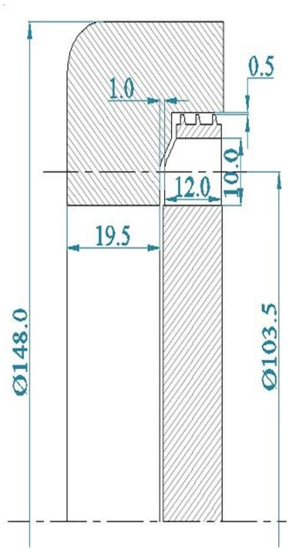

Figure 6. Modernized turbine stage CvM2R.

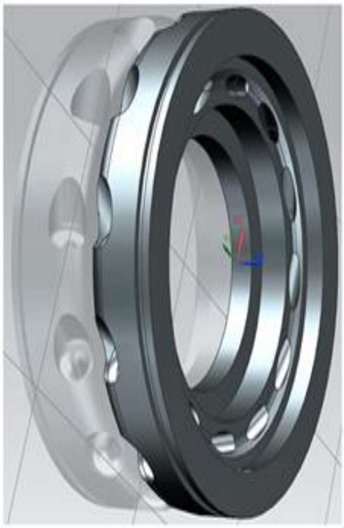

Figure 7. 3D model of the CvM2R stage SN.

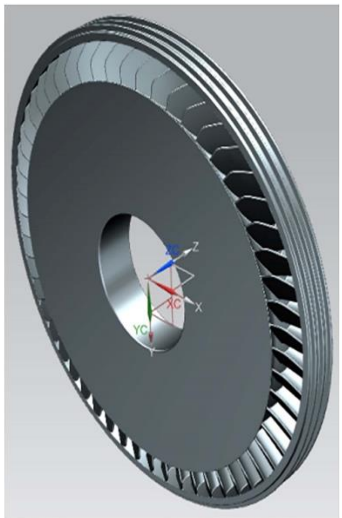

Figure 8. 3D model of the CvM2R stage wheel.

The modernized CvM2R stage maintains the main geometric characteristics of the CvMR stage. The basic principles of the flow range design in the stage under consideration are as follows: 1 – nozzle axes belong to a one-sheet hyperboloid of revolution, the neck whereof is located in the pitch diameter of the wheel blades at the beginning of the radiuses of concave wheel surfaces; 2 – wheel blades have leading edges that are elongated by increasing the blade width in the flow entrance direction by not more than 30% of the width of the original symmetric profile; 3 – the end surface of the SN outlet provides the necessary axial clearance size; 4 – the rooted surface reaches the nozzle axes; 5 – the peripheral part starts with the diameter of the wheel blades periphery; 6 – the taper surface connects them, while the radius of the taper and root surface equals the radius of the nozzle outlet; 7 – the mating taper-radius surface that limits the wheel blade edges is equidistant to the similar surface of the SN.

It is worth noting that in Cv stages, the blade has a ruled surface with parallel generating lines, runs through the centers of gravity of profiles, and belongs to the wheel radius. This shaping technique tilts the concave blade surface in the direction of the wheel revolution, which prevents the elongation of blades and facilitates flow towards the wheel periphery; therefore, the basic method was the design of the end surface of blades with radial rulings, which are widely used in turbines stages designed at the Leningrad Polytechnic University (Rassokhin, 2004).

The numerical experiment aimed at determining the effectiveness of CvMR (Figure 9a) and CvM2R (Figure 9b) stages (Kushchenko et al., 2015) enabled visualizing the WM flow at the SN inlet.

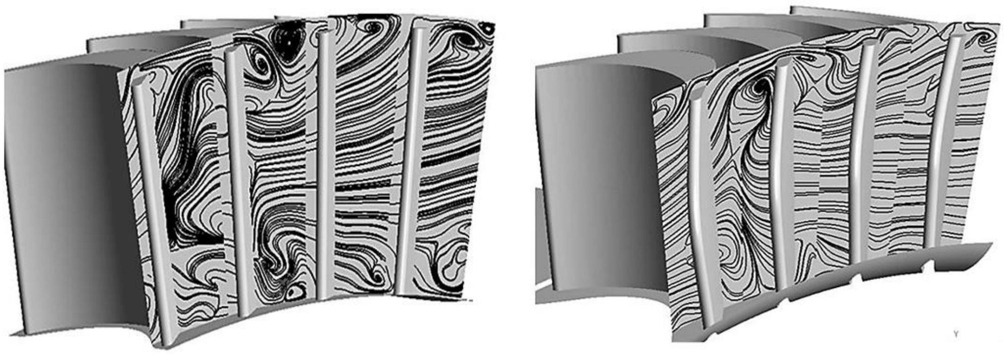

Figure 9. Comparison of stages, right to left – CvMR and CvM2R.

The comparison of stages shows that the CvM2R stage has the evenest flow at the wheel inlet, which, to a degree, increases its effectiveness by when compared to CvMR, where the relative gain in internal efficiency is:

$$\overline{\Delta\eta_B} = {\Delta\eta_B}/{\eta_B}. \qquad (1)$$

The wheel in a low emission axial active stage has an original construction that is presented in Figure 10. The construction consists of three details: plastic central part (2), which consists of integral disc, rotating blades, and shroud, as well as two steel bearing discs (1, 3). The torque is centered and transferred from the plastic part to the runner via steel discs. The plastic central part, manufactured via selective laser sintering, is fixed between the steel side discs with six bolts (4).

The described combined wheel construction is convenient for multivariate experimental studies and repairs at facilities that operate the rig. During the creation of the wheel, its geometry was optimized with regard to the results of strength calculations.

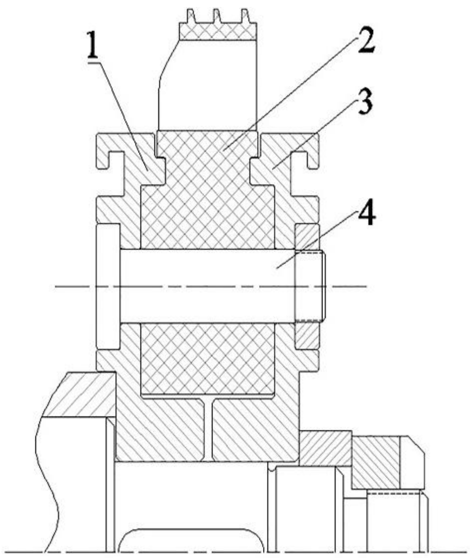

Figure 10. Wheel of the low emission active axial stage.

Strength calculations included the estimation of the stress state of the wheel construction elements from centrifugal loads with regard to axial bolt tension in the presence of friction across the contact surfaces of the steel and plastic central discs. Strength calculations were carried out via the finite element method using the ANSYS WB software ("Static structural" option).

The strength calculations for the compound wheel took into account the specific mechanical properties of the central disc material – plastic (Arzamasov & Makarova, 2005; Kushchenko et al., 2015). The main properties of plastic used in the calculations – PA12 polyamide – are presented in Table 1. (Operating temperature range of PA12 plastic is -40°C…90°C).

Table 1. The main properties of plastic used in the calculations.

Mechanical properties of PA12 plastic		
No.	Physical properties	Value
1	Specific weight, kg/m^3	1000
2	Stress limit, MPa	45
3	Elastic modulus, MPa	1400
4	Poisson's ratio	0.42
5	Friction against steel ratio	0.20

Raw data of strength calculations for the compound wheel:

1. Rotational speed of the wheel – 20000 rpm.
2. In order to make calculations quicker, strength calculations were performed for the a sector 1/12 the size of the disc, with a special boundary condition – slipping without friction against the plane – set for the two sides of the sector.
3. The thermal state of the wheel elements was ignored – all wheel elements had the same temperature of 20°C in the calculation.
4. The following contact conditions were set on the mating surfaces of the steel (side) and plastic (central) discs:
   a) the condition "contact with friction and possible reciprocal displacement of contacting surfaces, including partial disconnection" was set for the end surfaces of the plastic disc and the surface of bolt holes in the plastic disc (Bruyaka et al., 2013);
   b) the condition "integral contact without slipping" was set for the bolt holes in the steel side discs and the end surfaces of contact of tightened bolt heads (Bruyaka et al., 2013).

The contact in the central hole of the plastic disc was not taken into consideration.

Limitations in the use of the most accurate, but nonlinear model of type "a" contact were caused by the need to ensure an appropriate convergence of the numerical solution (Bruyaka et al., 2013). The increase in the preliminary axial compression of the bolt per 1/12 of the wheel was taken as 100 N. The geometry and results of strength calculations for one of the variants of the wheel are presented in Table 2.

Table 2. The main element that determines the strength of the entire wheel is the plastic disc.

Geometry and results of strength calculations for the wheel	
Wheel geometry	Stress state of the wheel
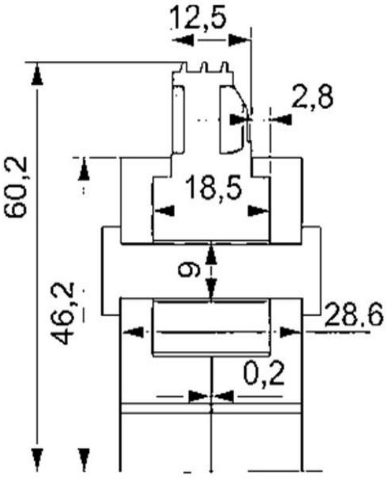	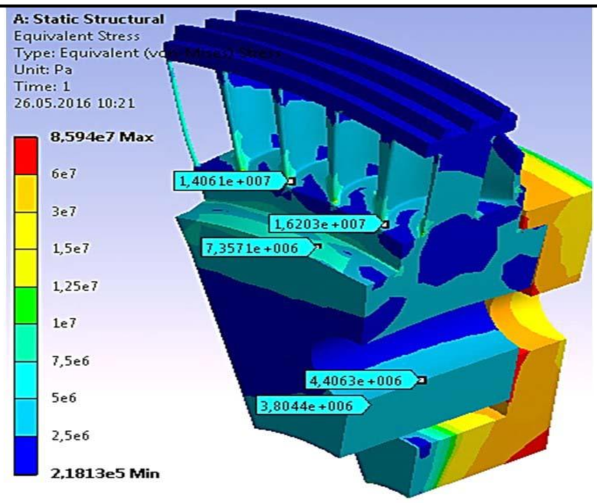

Note: clamp bolt diameter is 8 mm.

The main element that determines the strength of the entire wheel is the plastic disc – stress in the side steel discs are relatively small and do not exceed 100 MPa (Table 2).

The most stressed point in the plastic disc is located on the bolt hole surface – stress here reaches a level that is comparable to the yield point – 21 MPa. In order to demonstrate said area, it is necessary to show the results of centrifugal stress calculations for an autonomous plastic disc with main dimensions similar to the variant from Table 2.

A radical way to reduce said concentration of stress in the plastic disc is to use peripheral abutting shoulders on steel side discs (Figure 10 and Table 2). This design technique relieves the central part of the plastic wheel and centers it. The type of shoulder contact used in the calculation is "contact without a possibility of surface disconnection, but with possible low slipping" (Bruyaka et al., 2013). Maximum stress in the plastic disc for the improved wheel (with shoulders) is located on the surface of contact ledges, where the stress is 10…15 MPa (Table 2).

Strength properties of the construction material (plastic) have several essential features: the elastic modulus of plastic is 100 times smaller than that of steel; the Poisson's ratio of plastic is about 0.5 (Table 1). The latter feature produces a property that is rarely found in steel – virtually unalterable plastic disc volume during its deformation (Levin et al., 1981).

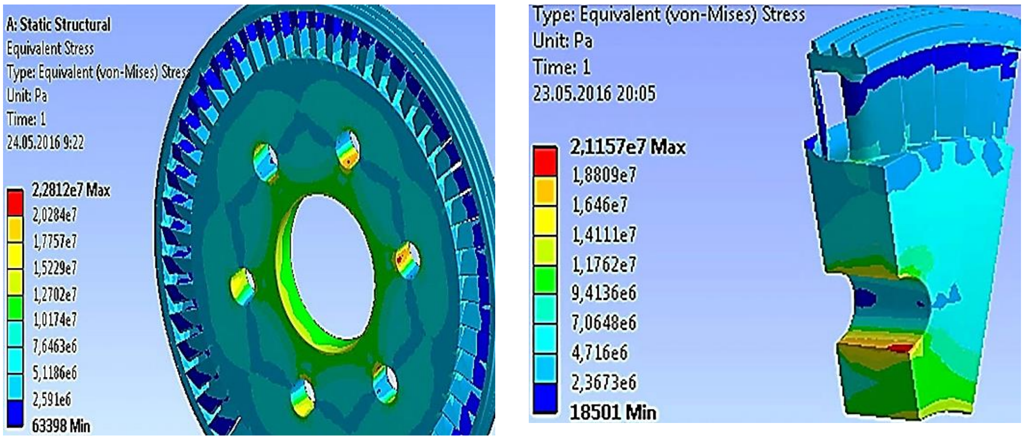

a) b)

Figure 11. Stress in the autonomous plastic disc: a) full disc; b) disc sector.

The described properties of plastic largely determine the features of the stress state of the plastic disc in the compound wheel. Figure 12 presents the obtained distribution of contact pressure across the end surface of the plastic disc. Calculation conditions: axial force of pretension was set at 100 N; rotational speed – 20000 rpm; coefficient of friction of two end contact surfaces of steel (side) and central (plastic) discs was set at 0.2. In the calculation, a guaranteed axial clearance was present between the steel discs (see Figure 10).

Discussion and Conclusion

Figure 12a shows a case without a clearance between the bolt and the respective hole in the plastic disc. Figure 12b shows a case with a 0.5 mm radial clearance between the bolt and the respective hole in the plastic disc.

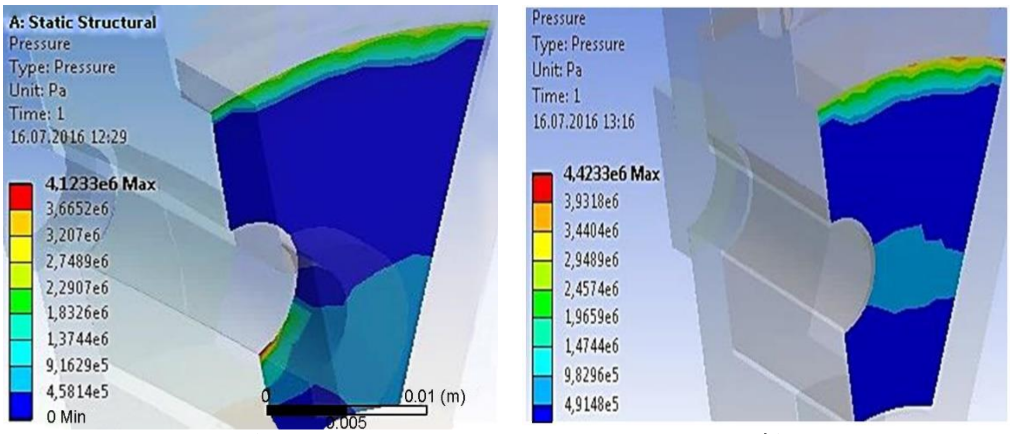

a) b)

Figure 12. Distribution of contact pressure across the end surface of the plastic disc: a) no clearance between the bolt and the hole in the plastic disc; b) 0.5 mm clearance between the bolt and the hole surface in the plastic disc.

Data presented in Figure 12 show that with other identical conditions, the area of significant contact pressure in the no-clearance variant is considerably larger than the one in the clearance variant. Differences in the contact areas can be explained by partial filling of free space in the clearance between the bolt and the hole with plastic without an increase in contact pressure (Figure 12b). This fact can be attributed to the abovementioned unalterable volume of plastic during deformation.

The ANSYS WB software enabled performing variants calculations for the stress state of the wheel under various bolt tension (Figure 13).

The geometric simulation model corresponds to the wheel variant from Table 2. The main input design parameter of R2 is maximum contact pressure on the circular abutting ledge of the plastic disc on the side of the leading edges of blades. The main and additional input parameters are as follows: R1 – bolt pretension force per 1/12 of the wheel and R3 – coefficient of friction across the end contact surfaces of wheel sector discs. The R1 value was set in the 0…1000 N range; the R3 value – in the 0.18…0.22 range (Kushchenko et al., 2015). The rotational speed of the runner in the calculation was set at 20000 rpm.

Results presented in Figure 13 show that the dependence of maximum contact pressure in the abutting ledge of the plastic disc on bolt tension is extreme.

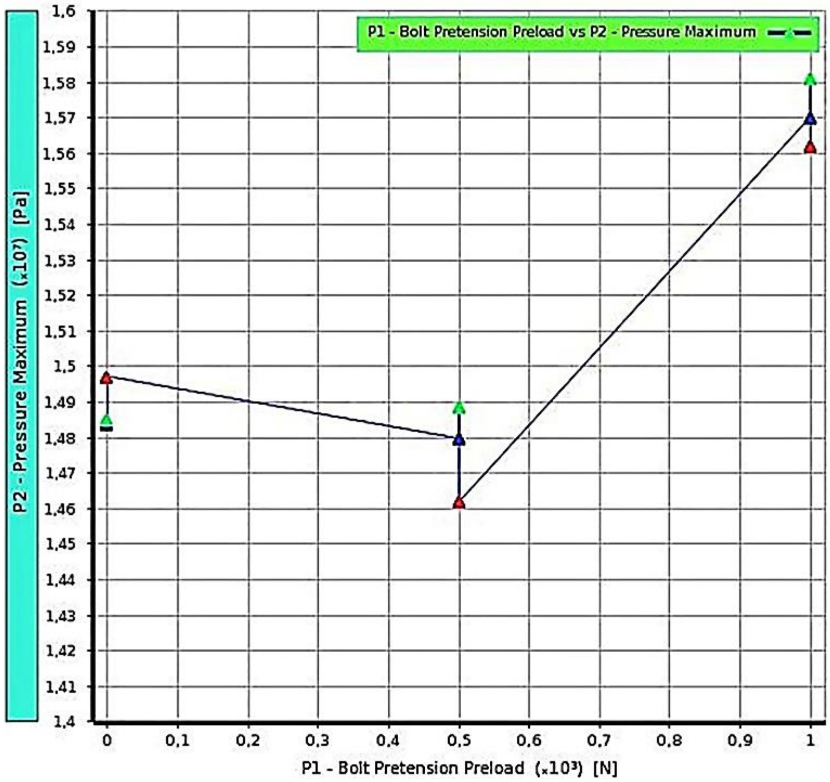

Figure 13. Dependence of maximum pressure in the contact ledge of the plastic disc at 20000 rpm on the bolt pretension preload (wheel variant from Table 2): red color corresponds to friction coefficient 0.22; blue – to 0.20; green – to 0.18.

It is necessary to rationalize the discovered dependence with regard to the following: increase in tension in the small value area (up to 300 N) increases contact pressure and area on the end surfaces of the plastic disc. The latter increases friction, which inhibits the centrifugal displacement of the disc and decreases contact pressure in the ledge. With higher bolt tensions (above 600 N), according to the described property of unalterable volume during deformation, axial compression of the plastic disc causes additional elongation of the disc in the centrifugal direction. The latter increases contact pressure on the ledge.

The discovered and rationalized dependence of pressure on the abutting ledge of the plastic disc on the bolt tension has practical implications.

Implications and Recommendations

The rationality of the design of the SN inlet via the offered method is confirmed by the numerical experiment. The effectiveness of the innovative technique, applied to the CvM2R stage, is achieved through advanced numerical methods of three-dimensional flow simulation using ANSYS software. The developed construction of a compound wheel with a plastic central disc has sufficient strength and can serve as an alternative material to steel. Using a wheel with circular abutting shoulders on steel side discs is reasonable. Using abutting contact shoulders in the plastic disc enables reducing the maximum stress in the disc by more than 25%.

A promising alternative to PA-12 plastic, which was chosen for the central disc in the above design, is the Accura Xtreme Plastic photopolymer (it has strength similar to polypropylene). Parts made of this plastic, manufactured using a 3D printer via stereolithography, have an improved quality of outer surfaces and increased stiffness (>20%). The operating temperature range of this plastic is -30°C…65°C.

Physical experiments are required to verify the results of numerical studies.

Disclosure statement

No potential conflict of interest was reported by the authors.

Notes on contributors

Gennadiy L. Rakov holds a Ph.D in Technical Science and now is an Assistant Professor at Peter the Great St. Petersburg Polytechnic University, Saint-Petersburg, Russia.

Victor A. Rassokhin holds a Doctor in Technical Science and now is a Professor at Peter the Great St. Petersburg Polytechnic University, Saint-Petersburg, Russia.

Nikolay A. Zabelin holds a Ph.D in Technical Science and now is a Director, Head of department at Peter the Great St. Petersburg Polytechnic University, Saint-Petersburg, Russia.

Sergey Yu. Olennikov holds a Ph.D in Technical Science and now is an Assistant Professor at Peter the Great St. Petersburg Polytechnic University, Saint-Petersburg, Russia.

Aleksandr A. Seeblev now is an Assistant Professor at Peter the Great St. Petersburg Polytechnic University, Saint-Petersburg, Russia.

Aleksandr I. Sukhanov holds a Ph.D in Technical Science and now is an Assistant Professor at Peter the Great St. Petersburg Polytechnic University, Saint-Petersburg, Russia.

Sergey M. Schislyaev holds a Ph.D in Technical Science and now is an Assistant Professor at Peter the Great St. Petersburg Polytechnic University, Saint-Petersburg, Russia.

References

Arzamasov, B.N. & Makarova V.I. et al. (2005). Materials science. M.: Bauman Moscow State Technical University. *Publishing house,* 648.

Bruyaka, V.A. et al. (2013). Engineering analysis in ansys workbench. Part 2. Study Guide. Samara. *Samara State Technical University,* 149.

Hagan, B. F. (2015). *Fluid transport system having divided transport tube:* USA patent 20150192072.

Hill, J. D. & Hill, S. J. (2016). *Apparatus and method for recovering off-gases from natural gas dehydrator:* USA patent 20160109121.

Imboccioli, C. & Bernardi, M. (2016). *Gas pressure regulator and method for piloting said pressure regulator:* USA patent 20160102811.

Khaleghi, S., Givehchi, S. & Karimi, S. (2013). Fuzzy risk assessment and categorization, based on event tree analysis (ETA) and layer of protection analysis (LOPA): case study in gas transport system. *World Applied Programming,* 3(9), 417-426.

Kirillov, I. I. (1972). *Turbomachine theory.* L.: Mechanical Engineering, 533.

Kuklina, N. I., Rakov, G. L. & Smirnov, M. V. (2015). Possibilities of improving the effectiveness of low emission active axial turbines. Materials of the 43rd International Scientific Forum "Peter the Great St. Petersburg Polytechnic University Science Week": Report Theses. *SPb.: Polytechnic University Publishing House,* 60-62.

Kushchenko, A. V. et al. (2015). Study on the coefficient of friction of rest of a polyamide coating against steel. *Modern high technologies,* 1, 42.

Levin, A. V., Borishansky, K. N. & Konson, Ye. D. (1981). Strength and vibration of blades and discs in steam turbines. *L.: Mechanical Engineering. Leningrad Branch,* 710.

Martens, C., Behrens, J. C. F. (2014). *Device and method for regulating the gas supply or the gas transport in a gas storage system:* USA patent 8770219.

Ogawa, H. et al. (2016). Performance Improvements in a Natural Gas Dual Fuel Compression Ignition Engine with 250 MPa Pilot Injection of Diesel Fuel as an Ignition Source. *SAE Technical Paper,* 2016-01-2306.

Pavel, V. Bulat & Vladimir N. Uskov. (2016). Gas-dynamic Waves and Discontinuities. *IEJME-Mathematics Education,* 11(5), 1101-1111.

Příhoda, M. et al. (2016). Heat output of the recuperator for preheating natural gas from a mobile container device. The meeting of departments of fluid mechanics and thermomechanics (35MDFMT): Proceedings of the 35th Meeting of Departments of Fluid Mechanics and Thermomechanics. *AIP Publishing,* 1768(1), 020016.

Rakov, G. L. (1982). Aerodynamic improvement of low emission turbines: PhD in Engineering dissertation. *L.: Leningrad Polytechnic Institute,* 137.

Rassokhin, V. A. (2004). Turbines designed at the Leningrad Polytechnic University: advantages, characteristics, and experience of design and operation. *Works of the Peter the Great St. Petersburg Polytechnic University,* 491, 152-161.

Shipovalov, A. N. et al. (2015). Development of energy-efficient technologies in the operation of underground gas storage facilities in a gas transport system. *Modern Problems of Science and Education,* 2-2.

Timm, M. L. et al. (2013). *Energy delivery system for a gas transport vessel containing low vapor pressure gas:* USA patent 8447175.

Xu, Y. et al. (2015). Research and application of dynamic reserves appraising methods in Sulige gas field under downhole throttling production mode. *International Field Exploration and Development Conference (IFEDC 2015), IET,* 1-3.

Yang, S. H., Long, W. & Gong, L. (2016). Analysis of micro vibration in gas film of aerostatic guide way based on molecule collision theory. MATEC Web of Conferences. *EDP Sciences,* 63, 02018.

Yao, J. et al. (2013). Numerical simulation of gas transport mechanisms in tight shale gas reservoirs. *Petroleum Science,* 10(4), 528-537.